Talanta 114 (2013) 152–159

Contents lists available at ScienceDirect

Talanta

journal homepage: www.elsevier.com/locate/talanta

Non-destructive analyses on a meteorite fragment that fell in the Madrid city centre in 1896

Javier Garcia-Guinea [a,*], Laura Tormo [a], Alvaro Rubio Ordoñez [b], Olga Garcia-Moreno [b]

[a] Dpto Geología, Museo Nacional de Ciencias Naturales (MNCN-CSIC), C/José Gutierrez Abascal 2, Madrid 28006, Spain
[b] Dpto Geología, Universidad de Oviedo, C/Jesus Arias de Velasco s/n, Oviedo 33005, Spain

ARTICLE INFO

Article history:
Received 5 October 2012
Received in revised form
21 March 2013
Accepted 28 March 2013
Available online 6 April 2013

Keywords:
Meteorite
Chondrite
Raman
Microanalysis
Tomography
Non-destructive
Troilite

ABSTRACT

The historical Madrid meteorite chondrite fell in 1896 showing thin melt veins with a 65% of brecciated forsterite fragments surrounded by a fine grained matrix formed by troilite, chromite and Fe–Ni blebs. It exhibits a delicate iron infill, neo-formation of troilite in pockets and shock veins and neo-formation of Na-feldspar formed at high temperature and fast quenching. The semi-quantitative mineral determinations were performed with IMAGEJ freeware and chemical mappings resulting in the following approximated compositions: olivine (~55%); augite (~10%); enstatite (~10%); plagioclase (~10%); chromite (~2%); troilite (~4%), kamacite–taenite α–γ-(Fe, Ni) (~7%) and merrillite (~7%). The specimen was also studied by computer tomography, micro-Raman spectroscopy and spectral cathodoluminescence. X-ray diffraction patterns were also recorded in non-destructive way on a polished surface because of the small size of the specimen. This combination of non-destructive techniques provides an improved knowledge on the Madrid-1896 meteorite compared to the previous study performed on the same specimen carried out twenty years ago by electron probe microanalysis and optical microscopy in destructive way. Limits of these techniques are the specimen's size in the analytical chambers and the threshold resolution of the microscopes analyzing shock veins micro-crystals.

1. Introduction

Historical meteorites kept in Museums are valuable stones that traditionally have been sliced to perform polished petrographic sections for their study under polarizing microscopes and by electron probe micro-analysis. Furthermore, at the present time, many different kinds of non-destructive techniques are being developed to analyze different valuable materials [1,2] by different facilities. Non-destructive evaluation methods usually include some kinds of microscopy and spectroscopy techniques to examine external surfaces of solids in detail [3]. The Madrid L6 chondrite historical fragment fallen in the Madrid downtown in 1896 was here studied only by non-destructive techniques together with measurements of electron probe microanalysis and X-ray diffraction (XRD) recorded in non-destructive way operating on the main polished plane of the meteorite. Madrid meteorite fragments were analyzed and studied in the same year of the fall (1896) [4,5]. It was a very important daylight fireball witnessed by hundreds of Madrid inhabitants together with their audible booms. The geological event was extensively reported allowing to outline nowadays a strewn field of fragments inside the Madrid city centre [6]. The Madrid meteorite was classified in 1985 [7] as a veined L6 chondrite and confirmed in 1990 [8] assuming the mineralogical composition of olivine (Fo_{76}), low-Ca pyroxene (Fs_{24}), metallic Fe, Ni (6%) veins and troilite (5 wt%) previously analyzed by Mason (1963) [9]. The Madrid meteorite was described in the 90s [10] under the polarizing microscope, as a severely shocked specimen, highly veined, i.e., with light-colored portions of the rock made up of silicates with undulated extinction being crossed by black shock veins. These veins consist of extremely fine-grained, shock-melted silicates and opaque minerals. The fine grain size is responsible for the dark appearance of the veins. The authors in [11] conclude that the Madrid meteorite is an impact-melt breccia exposed to at least two impact events: the first produced the melt (dark) portions from light material and was mixed with residual, unmelted, light material, i.e., formed the impact-melt breccia. The second impact event took place after the impact-melt breccia was assembled and solidified and resulted in the formation of the shock veins. Currently, the main Museums of Natural Science are setting new facilities to prevent irreversible damages to their main type specimens. Typically, they are micro-focus X-ray computer tomography (μCT), environmental scanning electron microscopes (ESEM) with large chambers to hold large specimens with analytical probes which provide different types of information such as (i) chemical data, i.e. wavelength dispersive spectroscopy (WDS), electron probe micro-analysis (EPMA), etc.; (ii) elemental analysis by energy dispersive spectroscopy (EDS), backscattering (BS), (iii) morphological, i.e., electronic, optical and X-ray imaging, (iv) molecular, i.e., micro-

* Corresponding author. Tel.: +34 91 4111328.
E-mail address: Javier.Garcia.Guinea@csic.es (J. Garcia-Guinea).

0039-9140/$ - see front matter © 2013 Elsevier B.V. All rights reserved.
http://dx.doi.org/10.1016/j.talanta.2013.03.070

Raman (Raman) and Infrared Transmission (FTIR) spectrometers in optical microscopes with large holders, (v) structural defects producing cathodoluminescence (CL) emission. These facilities provide a useful characterization of meteorite microstructural features good enough to infer crucial geological formation; in many cases much better than the simple observation performed under the traditional petrographic microscope. Operating with BS, EDS and WDS probes on poly-mineral specimens, such as a meteorite, it is important to state the chemical and elemental analyses accuracy adequately. For different metals such as iron–nickel alloys, or oxides, e.g., chromite, the EDS probe accuracy could be adequately compared to those provided by WDS or EPMA. Other interesting spectral comparison can be achieved with the cathodoluminescence (CL) and photoluminescence (PL) probes, the electron-beam excitation sources provide subtle different luminescence spectra compared with those provided from the most penetrative laser sources. The molecular information offered by the micro-Raman spectroscopy and integrated into an optical microscope provides a unique spectrum for each meteorite mineral grain of sub-micrometer dimensions. Meteorites encode important information on shock metamorphism which is a fundamental process in the evolution of the planetary bodies. They are materials particularly complex with long-time geological histories formed in the outer space which are studied with special emphasis on their micro-structures and micro-textures [12].

2. Experimental

2.1. Fireball and meteorite fragments

Madrid meteorite fragments fell in Madrid City Centre on February 10th in 1896, few seconds before 9:30 a.m. Ten samples were recovered in Madrid city, just after a bright white-blue light and a strong explosion scared and advertised people of the fallen meteorite [5]. The heaviest one weighs 143.79 g and the lightest 1.3 g. The meteorite fragments distribution formed a characteristic strewn field ellipse, NW/SE orientated. The largest meteorites fell in the NW orientation [6]. The material was highly crystallized and brecciated with chondrules poorly defined and clearly visible feldspars [6]. The Madrid L6 chondrite fragment, weighting 18.5 g and sized approximately $18 \times 17 \times 9\ mm^3$, belongs to the MNCN historical collection (Fig. 1a and b).

2.2. X-ray tomography

Following recent non-destructive modus operandi for meteorite fragments [13] we performed quantitative tomography analysis (μCT) of the meteorite (Fig. 1c and d). The stone was scanned with a Scanco micro-tomographic system housed at the National Research Centre for Human Evolution in Burgos, Spain (μCT 80, Scanco Medical, Switzerland), using the following settings for each scan: voltage 70 kV, amperage 114 mA, angular increment 0.36 grades and 0.8 s of time for each exposure. The μCT analysis of the sample was recorded during 4 h of X-ray exploration producing 640 planes with isometric voxel size of $36\ \mu m^3$ and three-dimensional views. The images were analyzed with Voxblast 3D software (Vaytek, Inc.) following the Conebeam Conv./Backpr mathematical method.

2.3. Chemical and elemental analyses on a flat surface

The historical specimen analyzed in this study was held into a mold of $29 \times 29\ mm^2$ together with wet bassanite ($CaSO_4 \cdot 0.5H_2O$). It was linked to metallic conductive plate to consolidate a solid block that was placed in the EPMA samples holder (Fig. 1b). This gypsum plaster can be removed by just washing to recover the historical specimen. The re-polished surface of the meteorite was examined by a combination of non-destructive facilities such as ESEM–EDS, CL, Raman and XRD. Analyses of morphology, textures, crystal habits and crystals sizes as well as the composition of glasses and minerals were collected using physical–chemical facilities of the Museo Nacional de Ciencias Naturales and the National Centre of Electron Microscopy of the Universidad Complutense, Madrid (Spain). Compositions of maskelenite glasses and meteorite crystals were obtained by EPMA. These data were performed with a WDS, JEOL-Superprobe JXA-8900M, equipped with four spectrometers and TAP, LD2, PETJ, LIF and LIFH crystal analyzers. The EPMA spot analyses were performed on the polished surface later sputtered with graphite. Analytical routine included the following oxides: SiO_2, TiO_2, Al_2O_3, FeO, MnO, MgO, CaO, Na_2O, K_2O, NiO and Cr_2O_3. The standards used were supplied by the Smithsonian Institute of Washington [1,11]. Measurement conditions for the meteorite minerals were 15 kV accelerating voltage and 20 nA beam current for mineral and 10 nA for the glass analyses in order to minimize sodium losses. This element was accordingly measured on the first position. The beam diameter used was 5 μm and the measurement times ranged from 10 to 60 s. Detection limits are in the order of 0.01 wt%. The environmental electron microscopy studies were performed using a FEI Inspect (5350 NE Dawson Creek Drive Hillsboro, Oregon 97124, USA) ESEM microscope. The ESEM in low vacuum mode admits hydrated samples to be studied in their original state, with the large field detector (LFD) to avoid electron losses. The samples were observed with the BS detector. The ESEM resolution at low-vacuum was at 4.0 nm at 30 kV (BS). The accelerating voltage was 200 V–30 kV and the probe current up to 2 μA was continuously adjusted; low vacuum was 0.45–0.55 Torr, with a working distance of 10 mm. Samples' EDS and mapping areas were studied with an energy dispersive X-ray spectrometer, Oxford Instruments INCA Energy 200 Energy Dispersive System.

2.4. X-ray diffraction on the flat surface

The XRD analyses of the Madrid meteorite surface were performed using XPOWDER software which also allows a full duplex control of the Philips PW-1710/00 diffractometer. The experimental conditions were set under CuKα radiation with a Ni filter and a setting of 40 kV and 40 mA. Performing background subtraction, Kα2 stripping and chemical elements were restrained to Si, Al, O, Ca, Mg, Ti, C, P; Fe, Mn, Ni, Cr, Cl, P, S, Na, K and Cr. These initial assumptions improve the Boolean search-matching on the ICDD-PDF2 and RRUFF databases.

2.5. Micro-Raman spectroscopy of meteorite minerals

The micro-Raman and photoluminescence spectra of the spot samples were performed in a Thermo-Fischer DXR Raman Microscope (West Palm Beach, FL 33407, USA). The system has Olympus BX-RLA2 Microscope and a CCD (1024×256 pixels) detector, motorized XY stage, auto-focus and microscope objectives Olympus UIS2 series (West Palm Beach, FL 33407, USA) all controlled through OMNIC 1.0 software. The light at 532 nm of a frequency doubled Nd:YVO_4 DPSS solid laser (maximum power 30 mW) was used for excitation. The DXR Raman has a point-and-shoot Raman capability of one micron spatial resolution. We used the 20 × objective of the confocal microscope together with the laser source at 532 nm and 6 mW in laser mode power at 100%. The average spectral resolution in the Raman shift ranging from 100 to 3600 cm^{-1} was 4 cm^{-1}, i.e., grating 900 lines/mm and 2 μm spot sizes. The system was operated under OMNIC 1.0 software fitting working conditions such as pinhole aperture of 25 μm, bleaching time 30 s; four exposures average timed 10 s each.

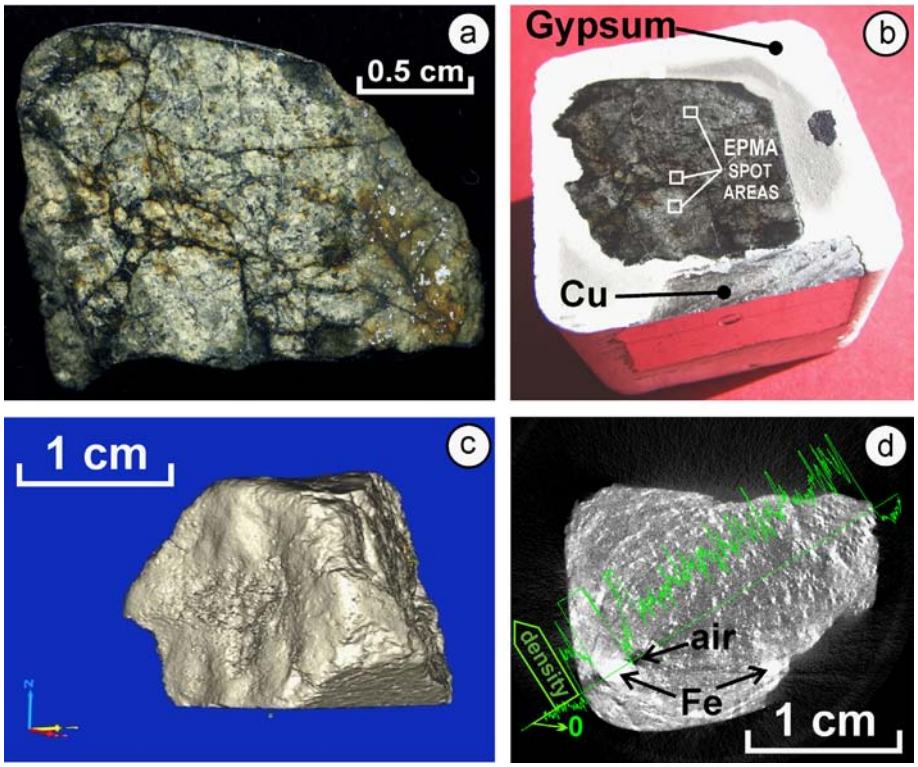

Fig. 1. The single fragment of Madrid L6 Chondrite of the Museo Nacional Ciencias Naturales (Madrid, Spain): (a) picture of the studied re-polished section, (b) the Madrid meteorite encased in a soluble plaster cast to be analyzed by electron microprobe, (c) three-dimensional image of the specimen taken by X-ray computerized tomography, and (d) one of the 640 CT-scan recorded sections exhibiting dense iron masses and empty air spaces.

2.6. Cathodoluminescence spectra and panchromatic plots of luminescent phases

The Inspect ESEM has a new coupled MONOCL3 Gatan probe to record CL spectra and panchromatic and monochromatic plots. It has a PA-3 photomultiplier tube covering a spectral range of 185–850 nm being more sensitive in the blue parts of the spectrum. A retractable parabolic diamond mirror and a photomultiplier tube were used to collect and amplify luminescence. The sample was positioned 16.2 mm beneath the bottom of the CL mirror assembly. The excitation for CL measurements was provided at 25 kV electron beam.

3. Results and discussion

3.1. Microfocus X-ray computer tomography of the meteorite body

A three-dimensional view of the scanned sample is shown in Fig. 1c and one of the 640 planes is shown in Fig. 1d. The planes show white areas of denser material, i.e. Fe–Ni, different gray tones for the silicates and black areas of probable air with zero gravity (Fig. 1d). Moreover, the morphology of the iron–air association matches alongside shock veins with characteristic shapes of pressure shadows observed in metamorphic rocks. These iron pressure shadows can be associated with the shock vein shear and extension fractures. The maximum compressive stress orientations following the pressure shadow geometry agree with the orientations derived from the fracture sets [14]. These non-destructive porosity measurements offer significant evidences to the physical processes that formed and modified the meteorites and their parent bodies [15].

3.2. Electron probe microanalyses of the mineral phases

The mineralogical EPMA average formulae with standard deviations of less than 3% are as follows: kamacite $Fe_{0.94}Ni_{0.06}$; taenite $Fe_{0.70}Ni_{0.30}$; nearly pure FeS troilite; chromite $Fe_{0.83}$ $Mg_{0.14}$ $Mn_{0.03}$ $(Cr_{1.58}$ $Al_{0.27}$ $Fe_{0.07}$ $Ti_{0.08})_2O_4$; olivine $Fe_{0.40-0.47}Mg_{1.52-1.55}Si_{0.99-1.02}O_4$ being a very constant composition of forsterite along the whole fragment; low-Ca pyroxene (enstatite) $(Mg_{1.54}Fe_{0.37})$ $Si_{1.98-2.01}O_6$; and a second Ca-rich pyroxene with an average formula of $(Ca_{0.69}Na_{0.07})$ $(Mg_{0.99}Fe^{2+}_{0.15}Al_{0.05}Fe^{3+}_{0.02}Ti_{0.01})$ $(Si_{1.97}Al_{0.03})_2$ O_6 (Fig. 2). Feldspar phases are oligoclase with low K contents $(Na_{0.80-0.88}Ca_{0.1}K_{0.04-0.08})Al_{1.12-1.16}Si_{2.86-2.89}O_8$ (Table 1 and Fig. 2). Table 1 displays some representative electron probe spot microanalyses performed with the silicates analytical routine of the JEOL software. Troilite (FeS); α–γ-(Fe, Ni) and merrillite $(Ca_{18}Na_2Mg_2(PO_4)_{14})$ were analyzed separately in the ESEM-EDS device. Analytical elemental and chemical maps and BS electron images obtained from both facilities, i.e., EPMA and ESEM-EDS BS photos were analyzed using IMAGEJ free software for the semi-quantitative determination of mineral phases. Noticeable difficulties detected in the process were the small size of grains in shock veins, the coexistence of common chemical elements in different minerals, e.g., calcium into augite and merrillite and chemical zonings in certain phases such as olivine with more and less iron contents. Finally, we suggest the following semi-quantitative general mineral determination: olivine (55%); augite (10%); enstatite (10%); plagioclase (10%); chromite (2%); troilite (~4%), kamacite–taenite α–γ-(Fe, Ni) (~ 7%) and merrillite (~ 7%). This is as far as we know the first modal composition proposed for all the mineral phases present in this chondrite the 5% missing could be attributed to porosity.

3.3. X-ray diffraction of the polished meteorite surface

The resultant XRD profile performed on the Madrid meteorite section studied by XPOWDER software suggests the following

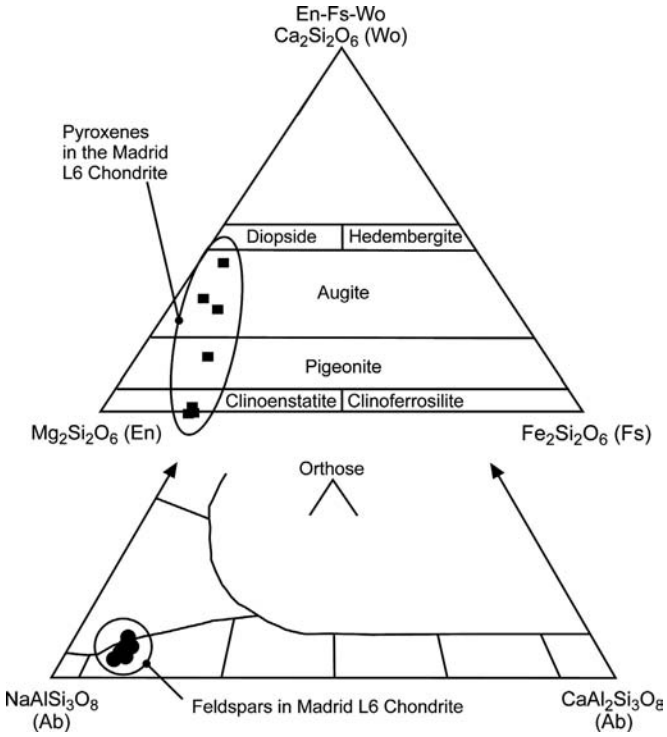

Fig. 2. Triangular diagrams of the chemical electron probe microanalyses data for the pyroxene and feldspar mineral groups.

Table 1
Electron probe microanalyses of the main minerals of the Madrid L6 chondrite.

Oxide	Olivine (55%)	Augite (10%)	Enstatite (10%)	Plagioclase (10%)	Chromite (2%)
SiO_2	38.85	54.74	55.64	64.92	0.14
Al_2O_3	0.0	0.64	0.19	21.56	5.92
FeO	21.15	6.61	13.16	0.33	28.87
MnO	0.03	0.0	0.0	0.0	0.96
CaO	0.03	15.77	0.90	2.17	0.01
TiO_2	0,0	0.37	0.21	0.02	2.80
P_2O_5	0.04	0.01	0.0	0.05	0.0
MgO	39.57	20.29	29.60	0.02	2.36
Na_2O	0.0	0.46	0.0	9.93	0.05
K_2O	0.0	0.02	0.0	0.83	0.01
NiO	0.02	0.0	0.14	0.04	0.05
Cr_2O_3	0.05	0.55	0.13	0.02	53.01
SO_3	0.04	0.02	0.01	0.01	0.0
Total	99.78	99.48	99.98	99.90	94.18

PDF2 card files: 72-2462 forsterite; 72-8574 Na-feldspar; 72-0431 enstatite; 72-0201 augite; 72-0877 taenite; 72-0645 kamacite. Semi-quantitative XRD values are roughly approximated since they were calculated from the XRD peaks obtained from an oriented surface compared to other improved analyses recorded in destructive mode from pulverized chondritic material (Fig. 3a).

3.4. Micro-Raman spectroscopy of isochemical compounds

One of the most useful applications of the Raman technique applied to meteorite Science is to distinguish among isochemical $CaPO_4$ phases such as apatite and merrillite. Fig. 3b depicts a characteristic Raman spectrum of merrillite recorded in a grain of Ca-phosphate previously analyzed with the chemical and elemental probes. It exhibits the large Raman peaks split at 957 and 971 cm^{-1} which dominate the spectrum. These bands originate from the ν_1 symmetric stretching mode of $(PO_4)^{3-}$ ions bands of intermediate intensity at 1036 and 1071 cm^{-1}. These bands are the result from

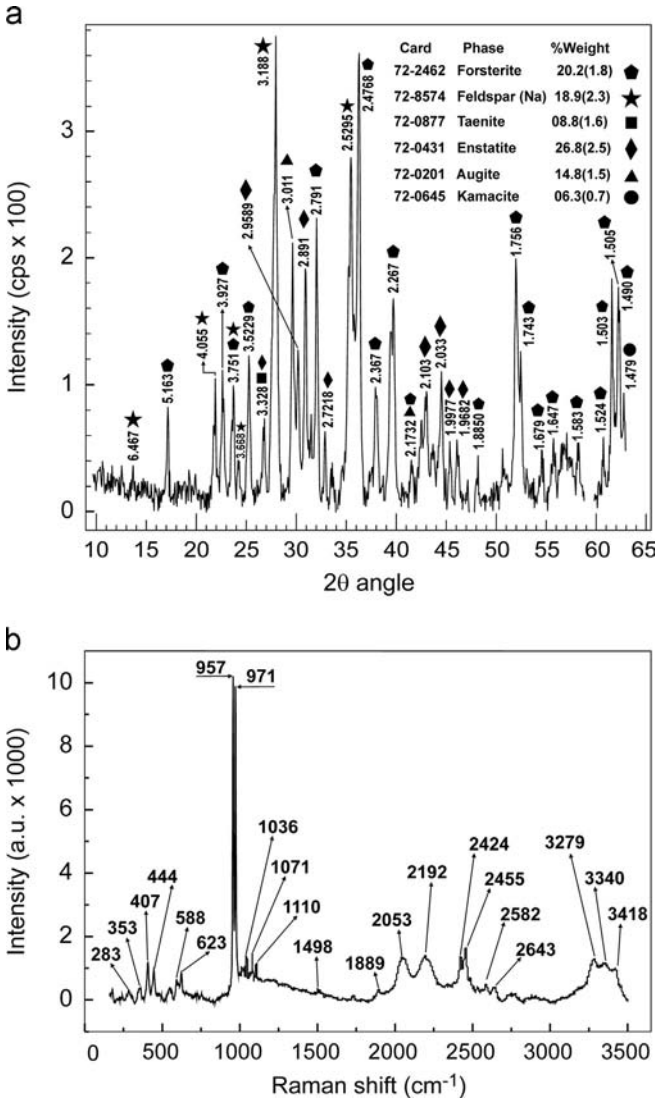

Fig. 3. (a) X-ray diffraction profile obtained from the polished face of the meteorite and (b) Raman spectrum of a merrillite grain sized 200 μm.

antisymmetric ν_3 vibrations [16]. Additional bands at lower wave numbers, 174, 407, and 444(4) cm^{-1}, could also be assigned to the merrillite phase [17]. The experimental merrillite Raman spectrum also displays a spectral region from 1500 to 3500 cm^{-1} with photoluminescent features such as those observed at 2053 and 2192 cm^{-1} which can also be assigned to substitutional REE elements in structural Ca^{2+} positions of the merrillite crystallographic structure.

3.5. ESEM-EDS-CL study of microstructures

Fig. 4a displays elemental data recorded with the BS probe on a pocket with coupled grains of merrillite, Na-feldspar and Fe–Ni phases surrounded by olivine matrix. Merrillite grains display significant amounts of REE such as Nd 0.11–0.16% and Dy 0.06% (Table 2) which may be responsible for the photoluminescence activators in the extended region of the Raman spectrum. In addition, Fig. 4a includes spot positions of the EDS elemental analyses included in Table 2. The suggested normative mineral inferred from the elemental EDS analyses is also shown in Table 2. Semi-quantitative modal mineral analyses were calculated approximately by a combination of partial EDS chemical mappings and BS image analyses with ImageJ freeware.

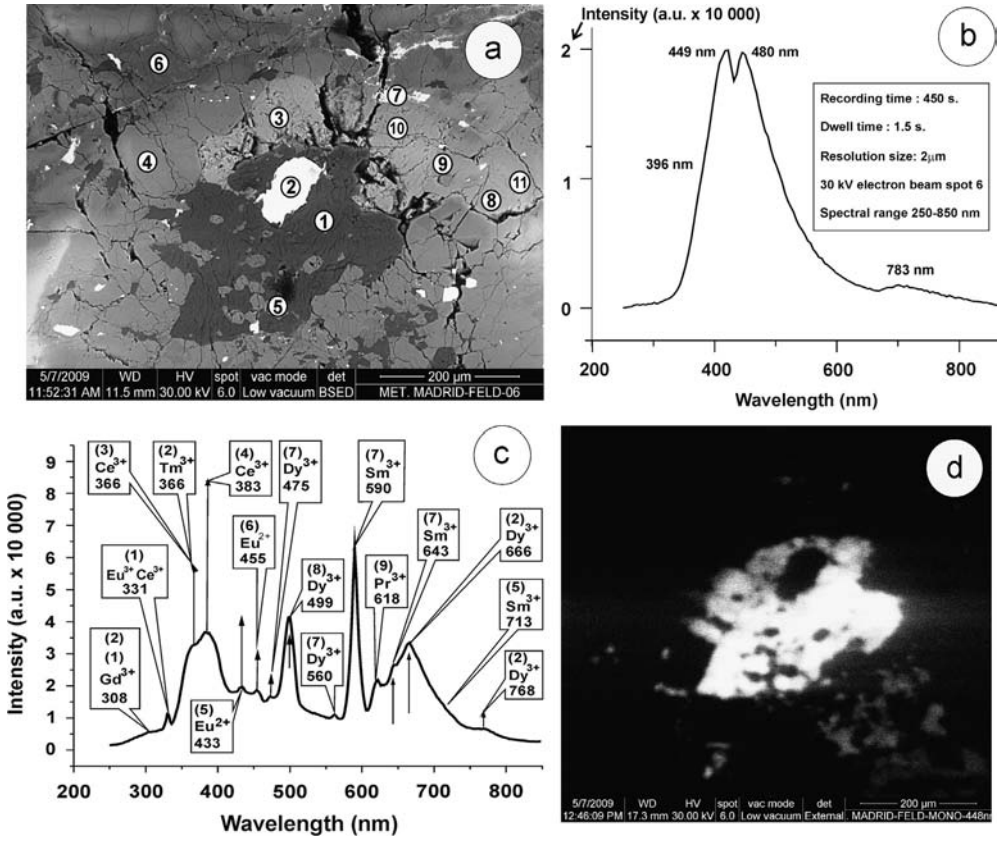

Fig. 4. Energy dispersive spectroscopy analyses of the Madrid meteorite on a zone rich in Na-feldspar and merrillite: (a) spot positions of the experimental EDS elemental analyses, (b) cathodoluminescence spectrum of a plagioclase crystal, (c) cathodoluminescence spectrum of a merrillite crystal with the defect-emission assignations attributed to different REE ions, and (d) monochromatic plot at 448 nm of the plagioclase crystal showing a strong spectral CL blue emission (20,000 a.u.).

Table 2
Chemical analyses performed by X-ray energy dispersive spectrometry in the Environmental Scanning Electron Microscope on the spots placed in Fig. 4.

Spot no. Element	1 Weight (%)	2 Weight (%)	3 Weight (%)	4 Weight (%)	5 Weight (%)	6 Weight (%)	7 Weight (%)	8 Weight (%)	9 Weight (%)	10 Weight (%)	11 Weight (%)
Na K	6.22	0.0	0.67	0.0	0.96	0.0	0.0	2.02	1.98	0.56	1.60
Mg K	1.18	1.75	1.50	22.26	19.79	16.22	1.95	3.24	3.02	1.27	3.32
Al K	9.76	0.84	0.21	0.52	1.39	0.36	0.39	0.21	0.27	0.21	0.25
Si K	29.11	3.18	1.93	19.75	19.74	25.47	1.83	1.85	1.59	1.63	2.02
P K	0.87	0.49	17.99	0.0	0.33	0.0	1.55	20.21	19.97	17.46	20.19
S K	0.0	0.0	0.0	0.0	0.24	0.26	21.05	0.0	0.0	0.34	0.0
Cl K	0.0	0.19	4.81	0.0	0.0	0.0	0.0	0.16	0.27	4.89	0.0
K K	0.97	0.0	0.0	0.0	0.0	0.0	0.0	0.13	0.19	0.12	0.13
Ca K	2.01	0.64	30.52	0.44	0.41	0.90	2.99	26.90	27.91	31.86	26.79
Mn K	0.0	0.0	0.0	0.36	0.31	0.34	0.0	0.0	0.0	0.0	0.0
Fe K	1.90	43.82	2.18	13.14	13.25	10.94	36.95	2.19	2.04	2.18	2.38
Ni K	0.20	18.74	0.18	0.0	0.0	0.16	0.0	0.0	0.0	0.0	0.13
Nd L	0.0	0.0	0.0	0.0	0.0	0.0	0.0	0.16	0.11	0.0	0.07
Dy L	0.0	0.0	0.0	0.0	0.0	0.0	0.0	0.0	0.06	0.0	0.0
Calc. Oxygen	47.78	30.35	40.01	43.53	43.58	45.35	33.29	42.93	42.59	39.48	43.12
Totals	100	100	100	100	100	100	100	100	100	100	100
Mineral inferred	Oligoclase	Kamacite	Merrillite	Olivine	Olivine	Augite	Troilite	Merrillite	Merrillite	Apatite	Merrillite

Complementarily, we also performed selective spectral cathodoluminescence (Fig. 4b and c) and monochromatic plots, e.g., Fig. 4d, to gain knowledge about the spatially resolved distribution of the REE luminescence activators in several mineral phases of the meteorite. The monochromatic plot at 448 nm of Fig. 4d is associated with the strong spectral CL blue emission (20,000 a.u.) of plagioclase represented in Fig. 4b.

Fig. 4c includes both, the experimental CL spectrum of merrillite (spot 3 in Fig. 4a) together with the defect-emission assignations attributed to different REE ions of Blanc et al. [18]. Fig. 5 is a composition of four ESEM images exhibiting selected textural and micro-structural features in the L6 chondrite. Fig. 5a displays a chondrite area with different morphological types of forsterite crystals, such as the characteristic elongated-parallel olivine lamellae or isometric grains found together with Fe–Ni masses and plagioclase fillings. Fig. 5b shows a detail of a shock vein with brecciate forsterite fragments of very variable sizes mixed with spherical Fe–Ni metal/iron sulfide globules and masses of Fe–Ni alloy, embedded into a silicate glass matrix. This composition of the shock veins in L6 chondrites reveals non-equilibrium melts with high FeO(T) contents compared to non-melted silicates. The iron redistribution between metal and silicate liquids took place at some stage in the shock episode; the

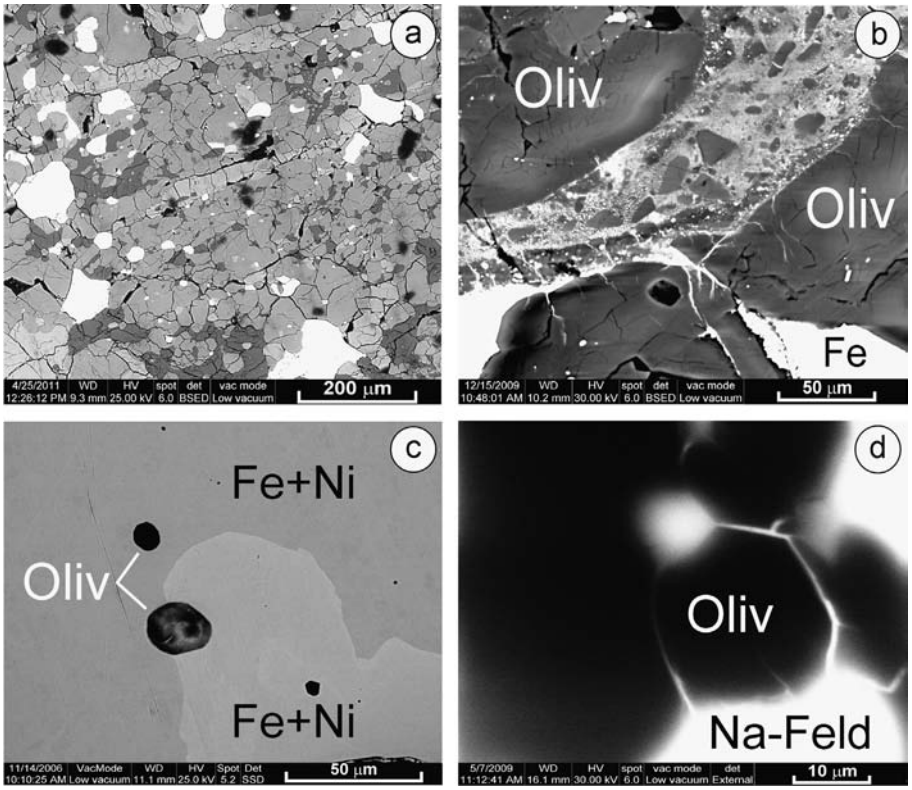

Fig. 5. ESEM images of several areas of the Madrid meteorite: (a) chondrule with parallel olivine (BS image), (b) shock vein with matrix and brecciated forsterite and micro-veins of Fe–Ni (BS image), (c) kamacite–taenite Fe–Ni mass including forsterite relicts (BS image), and (d) panchromatic CL image highlighting the thin intrusion of Na-feldspar through olivine fissures.

olivine of the host neighboring walls display variable gray-tones zoning with different iron contents. Fig. 5c shows a detail of near-spherical forsterite rounded-grains dissolved into a mixed taenite and kamacite matrix. Forsterite is a refractory mineral with a melting point ca. 1850 °C accordingly; both observations suggest high temperatures for the iron diffusion. Fig. 5d shows a panchromatic CL image of this infill micro-texture showing non-luminescent olivine crystals together with strongly cathodoluminescent Na-feldspar. This photo has enough resolution to observe the delicate feldspar infill into very thin forsterite inter-phases; that observation suggests high temperature for the feldspar diffusion processes into the meteorite chondrite matrix. The Fe–Ni masses observed into the shock veins could be very skinny being visible in the fissuring system among olivine grains and forming bubbling drops into the vein matrix.

Performing one by one chemical analysis spots with the ESEM-EDS probe we obtained (Fig. 6a) a mineralogical–chemical graphical scheme, including shock vein, iron pocket, mineralogy and chemical variations under the BS suggesting two genetic processes: (1) iron fluid injection and (2) late hot H_2S gas infill or internal S exsolution from the silicate melt. Fig. 6b and c depicts EDS line-scan plots detailing the composition along the shock vein walls. Fig. 6d shows other EDS line-scan recorded in a forsterite–merrillite boundary depicting chemical variations inside the $CaPO_4$ mass. We observed a chemical anomaly of C sighted at 25 μm from the grain boundary in which Ca and P decrease. That datum suggests a merrillite zoning formed in several stages, one of them involving a genetic environment temporally enriched in carbon phases, e.g., CH_4 gas.

4. Meteorite formation processes

The Madrid chondrite is a moderate shock-metamorphosed stone meteorite classified correctly as an ordinary L6 chondrite [8,9]. Madrid specimen shows thin melt veins sized from 0.02 up to 0.08 mm in width with a 65% of brecciate forsterite fragments in the frontier of resolution threshold of ESEM and EPMA microscopes. These melted areas, formed under high-pressure, high temperature and dynamic shock conditions, consist of spherical Fe–Ni metal/iron sulfide globules embedded into a silicate glass matrix, showing that the melt was quenched at high cooling rate. The Fe–Ni fraction in the globules has two phases, composed of a bcc phase (~5 wt% Ni) and an fcc phase (~49 wt% Ni), indicating that fractional crystallization of the metal occurred during fast cooling [19]. The EDS elemental analysis number 2 (Table 2) of this matrix shows 62.64% FeO(T) and 23.83% NiO with 2.90% MgO and 6.81% SiO_2 6.81%. It is very common that the metal fraction contains appreciable amounts of non-siderophile elements such as Si, Mg and O suggesting these elements were trapped in the metal, either as alloying components or as tiny silicate or oxide inclusions. The composition of the silicate glass in shock veins of the L6 chondrites reveals non-equilibrium melting of some silicate phases; they show high FeO(T) contents compared to the contents observed in non-melted silicates. The iron redistribution between metal and silicate liquids took place during the shock event. These silicate glasses contain minute iron sulfide precipitates exsolved by quenching, suggesting that the molten silicate retained significant amounts of S, dissolved at high temperature and high pressure [20]. The meteorite sample shows also Na-rich feldspars scarcely observed in similar L6 chondrites, which used to be more Ca-rich [21,22]. The anomalies in the Na content could be explained by the preferential melting of plagioclase which occupies spaces between the other better crystallized minerals or by trapping Na vapor coming from a hotter zone into the cooler regions in contact with these un-melted silicates. Sodium distributions in olivine and melt inclusions are studied in chondrules, both in the mesostasis and bulk chondrule. The distribution can give an idea of the interactions with ambient gas during meteoritic chondrule formation [23]. This hypothesis is in good agreement with the observed delicate iron micro-structure infill of the Madrid

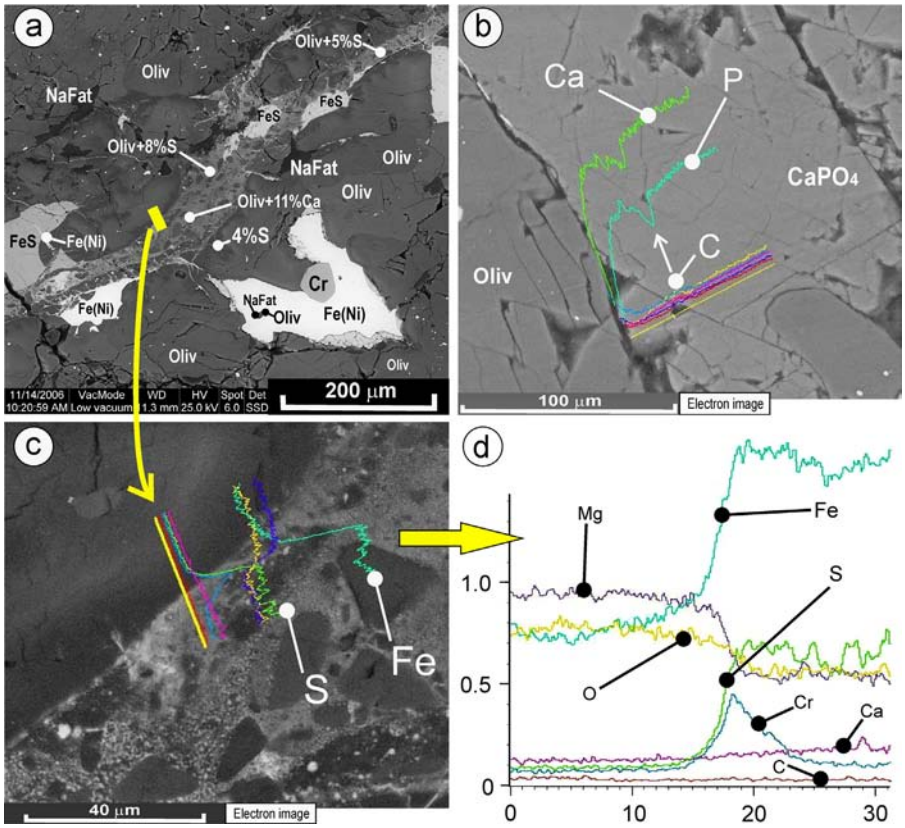

Fig. 6. (a) Shock vein with a fine grained matrix and brecciated forsterite showing details of the chemical distribution of the sulfur element, micro-textures, mineralogical composition and chemical EDS line-scan position. (b) Chemical EDS line-scan from the forsterite host to the vein matrix with more S and Fe. (c) Detail of the EDS line-scan for the different chemical elements. (d) A second EDS line-scan performed into a merrillite grain with a carbon-rich growing layer.

meteorite, typically formed at high temperature and quenching. Concerning the iron sulfide content observed in silicate glass of the shock veins in the Madrid meteorite, it is richer in S compared to the average bulk composition of a standard L-chondrite having a preferential incorporation of S in the melt. Chondrites with higher shock levels, such as the Madrid L6 chondrite case, show melt droplets of Fe–Ni metal and troilite (FeS) whose composition and abundance correspond to the maximum equilibrium shock state achieved by the sample. At these higher shock levels, the abundance of other shock-induced features, such as polycrystalline kamacite, sheared and bubbling troilite, polycrystalline troilite and poly-mineral melt veins, serves as textural criteria that can be used to establish peak-shock conditions. All of these features serve as aids for shock classifying L chondrites as well as for quantifying minimum peak temperatures that resulted during shock metamorphism [24]. The silicate glass is enriched in Si, Al, Ca and Na, showing a preferential incorporation of plagioclase in the melt due to the lower melting point of Na-feldspars. The high sulfur content analyzed in the silicate matrix together with the polycrystalline troilite kamacite micro-crystals could be explained by the characteristic fast kinetics of metal-sulfide reactions. Fast cooling produces textural changes in adjoined metal-troilite grains during post-impact metamorphism of these shock veins, whereas slow rate of silicate reactions causes them to be either unaffected or only partially annealed, except in the largest impact events [25].

5. Conclusions

Although the classification scheme of the Madrid-1896 L6 chondrite was properly established in previous publications, the semi-quantitative mineral modal percentage determinations are first presented in this study. They are inferred from elemental and chemical spot analyses obtained by EPMA and SEM–EDS techniques, together with imaging analysis by IMAGEJ freeware of the BS and chemical mapping images, suggesting the following approximated composition: olivine (~55%); augite (~10%); enstatite (~10%); plagioclase (~10%); chromite (~2%); troilite (~4%), kamacite–taenite α–γ-(Fe, Ni) (~7%) and merrillite (~7%). These new microscopes with large holding sample chambers allow analyzing historical meteorites in a non-destructive way obtaining high resolution images, accurate chemical spot analyses, high sensitivity cathodoluminescent spectra and chromatic luminescence images. Raman spectra of isochemical phases provide different molecular information allowing individual mineralogical identification of grains of just a few microns. Traditional complementary techniques, such as X-ray diffraction and electron probe microanalyses can be used successfully in a non-destructive way only for small specimens previously sliced. The experimental results described here significantly broaden previously published knowledge on the L6 Chondrite Madrid (Fall 1896) which was obtained by destructive techniques such as electron probe microanalysis and optical microscopy which destroy an important part of the historical specimen obtained in 1990. Three features linked with the shock veins are as follows: (1) flimsy iron infill, (2) neo-formation of iron sulfide phases in pockets and shock veins and (3) neo-formation of Na-feldspar. The mineralogical composition of the silicate matrix into shock veins mixed together with polycrystalline troilite kamacite micro-crystals, micro-droplets and other micro-textural features points to the shock metamorphism nature of the Madrid L6 chondrite.

Acknowledgments

We are grateful to the Spanish project CGL2010-17108 and to Rafael Gonzalez Martin for the X-ray diffraction recordings and interpretation of the profiles.

References

[1] B. Schrader, H. Schulz, G.N. Andreev, H.H. Klump, J. Sawatzki, Talanta 53 (2000) 35.
[2] D.N. Papadopoulou, G.A. Zachariadis, A.N. Anthemidis, N.C. Tsirliganis J.A. Stratis, Talanta 68 (2006) 1692.
[3] C. Hellier (Ed.), McGraw-Hill, New York, US, ISBN 0-07-028121-1.
[4] S. Calderon y Arana, Le Nat. 216 (1896) 55.
[5] A.F. Gredilla y Gauna, Anal. Soc. Esp. Hist. Nat. Actas 25 (1896) 223.
[6] L. Alcala, C. Martin Escorza, Bol. R. Soc. Esp. Hist. Nat. XII Bienal. Tomo. Extr. 125 (1996) 471.
[7] A.L. Graham, A.W.R. Bevan, R. Hutchison, Catalogue of Meteorites, 4th Edition, British Museum, Tucson, Arizona, 1985.
[8] I. Casanova, K. Keil, R. Wieler, A. San Miguel, E.A. King, Meteoritics 25 (1990) 127.
[9] B. Mason, Geochim. Cosmochim. Acta 27 (1963) 1011.
[10] E.J. Jarosevich, J.A. Nelen, J.A. Norberg, Geostand. Newslett. 4 (1980) 87.
[11] E.J. Jarosevich, L.A. Boatner, Geostand. Newslett. 15 (1991) 397.
[12] A. Bischoff, D. Stöffler, Eur. J. Mineral. 4 (1992) 707.
[13] M. Uesugi, K. Uesugi, M. Oka, Earth Planet. Sci. Lett. 299 (2010) 359.
[14] A.R. Burger, B.E. Perry, B. White, Am. Mineral. 55 (1970) 1791.
[15] G.J. Consolmagno, D.T. Britt, R.J. Macke, Chem. Erde-Geochem. 68 (2008) 1.
[16] R.W. Mooney, S.Z. Toma, R.L. Goldsmith, K.H. Butler, J. Inorg. Nucl. Chem. 30 (1968) 1669.
[17] T.F. Cooney, E.R.D. Scott, A.N. Krot, S.K. Sharma, A. Yamaguchi, Am. Mineral. 84 (1999) 1569.
[18] P. Blanc, F. Baumer, F. Cesbron, D. Ohnenstetter, G. Panczer, G. Remond, in: M. Pagel, V. Barbin, P. Blanc, D. Ohnenstetter (Eds.), Cathodoluminescence in Geosciences, Springer Verlag Berlin, 2000, pp. 127–160.
[19] H. Leroux, J.C. Doukhan, F. Guyot, Earth Planet. Sci. Lett. 179 (3) (2000) 477.
[20] J. Llorca, J.M. Trigo-Rodriguez, J.L. Ortiz, J.A. Docobo, J. Garcia-Guinea, A.J. Castro-Tirado, A.E. Rubin, O. Eugster, W. Edwards, M. LaubensteinI. Casanova, Meteorit. Planet. Sci. 40 (2005) 795.
[21] V. Correcher, L. Sanchez-Muñoz, J. Garcia-Guinea, A. Delgado, NIM Sect. A 580 (2007) 637.
[22] J. Garcia-Guinea, L. Sanchez-Muñoz, L. Tormo, E. Crespo-Feo, J. Ruiz, A.I. Martin-Herrero, A. Cremades, AIP Conference Proceedings 1163, 141 (Corals I) Mainz, Germany, 2–4 April 2009.
[23] R.H. Hewins, B. Zanda, C. Bendersky, Geochim. Cosmochim. Acta 78 (2012) 1.
[24] M.E. Bennett III, H.Y. McSween Jr., Meteorit. Planet. Sci. 31 (1996) 255.
[25] A.G. Tomkins, Meteorit. Planet. Sci. 44 (2009) 1133.